

Suppression of alpha-induced lateral surface events in the COBRA experiment using CdZnTe detectors with an instrumented guard-ring electrode

The COBRA collaboration

J.-H. Arling^{a,b} M. Gerhardt^a C. Gößling^a D. Gehre^c R. Klingenberg^a K. Kröninger^a
 C. Nitsch^a T. Quante^a K. Rohatsch^c J. Tebrügge^{a,1} R. Temminghoff^a R. Theinert^a
 S. Zatschler^c K. Zuber^c

^a*Technische Universität Dortmund, Lehrstuhl für Experimentelle Physik IV, Otto-Hahn-Str. 4a, 44221 Dortmund*

^b*now at Deutsches Elektronen-Synchrotron DESY, Hamburg*

^c*Technische Universität Dresden, Institut für Kern- und Teilchenphysik, Zellescher Weg 19, 01069 Dresden*

E-mail: jan.tebruegge@tu-dortmund.de

ABSTRACT: The COBRA collaboration searches for neutrinoless double beta-decay ($0\nu\beta\beta$ -decay) using CdZnTe semiconductor detectors with a coplanar-grid readout and a surrounding guard-ring structure. The operation of the COBRA demonstrator at the Gran Sasso underground laboratory (LNGS) indicates that alpha-induced lateral surface events are the dominant source of background events. By instrumenting the guard-ring electrode it is possible to suppress this type of background. In laboratory measurements this method achieved a suppression factor of alpha-induced lateral surface events of 5300^{+2660}_{-1380} , while retaining $(85.3 \pm 0.1) \%$ of gamma events occurring in the entire detector volume. This suppression is superior to the pulse-shape analysis methods used so far in COBRA by three orders of magnitude.

KEYWORDS: CZT, CdZnTe, semiconductor detector, coplanar-grid, guard ring, background suppression, surface events

¹Corresponding author

Contents

1	Introduction	1
2	Guard ring instrumentation of CdZnTe detectors	2
3	Charge-cloud dynamics of alpha particles	3
4	Predictions from an electric-field calculation	4
5	Experimental setup	6
6	Measurements and results	7
7	Summary and outlook	9

1 Introduction

The COBRA (CdZnTe **0** Neutrino Double **B**eta **R**esearch **A**pparatus) collaboration [1] searches for neutrinoless double beta-decay ($0\nu\beta\beta$ -decay) [2]. This decay is forbidden in the Standard Model of particle physics. The quest for lepton-number violation is a main motivation to search for $0\nu\beta\beta$ -decay. Furthermore, the detection of this process could give information about several general properties of neutrinos like the neutrino mass scale and mass hierarchy. The decay has not been measured yet, limits on the half-life are of the order of 10^{25} yr, depending on the nuclide under study [3–5]. Special experimental techniques are required to measure such rare decays. One crucial issue is the reduction of background events which can mimic the searched-for decay, coining the term ‘low-background experiment’.

The COBRA collaboration operates a demonstrator setup at the Gran Sasso underground laboratory (Italy), technical details can be found in Ref. [6]. The demonstrator consists of 64 CdZnTe coplanar-grid (CPG) semiconductor detectors with the volume of 1 cm^3 each. CdZnTe contains nine nuclides that can undergo double beta-decays: ^{64}Zn , ^{70}Zn , ^{106}Cd , ^{108}Cd , ^{114}Cd , ^{116}Cd , ^{120}Te , ^{128}Te and ^{130}Te . Due to its high Q -value of 2 814 keV [7], ^{116}Cd is the most promising candidate for the COBRA experiment. No significant excess over the estimated background was found which results in half-life limits of about 10^{21} yr for the ground-state to ground-state $0\nu\beta^-\beta^-$ transitions of ^{70}Zn , ^{114}Cd , ^{116}Cd , ^{128}Te and ^{130}Te as documented in Ref. [8]. One conclusion drawn from the operation of the demonstrator is that the main background component stems from alpha-induced lateral surface events. In the current scheme, lateral surface events are identified by analyzing the recorded pulse shapes in the detector; details of this method can be found in Ref. [9].

All detectors used by COBRA feature a guard ring, which is a boundary electrode surrounding the CPG anodes. It is a common method to improve the detector performance, as it leads to a better balanced weighting potential [10] and to a reduction of leakage currents. In the current

configuration, the guard ring is not instrumented and left on a floating potential. Setting a defined potential on a guard-ring structure to suppress surface events was studied in Ref. [11] using Germanium detectors. First measurements have shown that this novel method can be used for the COBRA detectors as well without deteriorating the detector performance significantly [12]. This paper discusses the instrumentation of guard rings for large 6 cm^3 detectors used for the upgrade of the COBRA demonstrator.

2 Guard ring instrumentation of CdZnTe detectors

In CdZnTe, the product of lifetime and mobility for electrons and holes is different by three orders of magnitude, introducing a strong interaction-depth dependence of the detectors response. To compensate for this effect, the so-called coplanar-grid technology [13] is used in COBRA. It is a single-polarity charge-carrier sensing method, where in this case only the electron signal is read out. In this technique, two anodes are comb-shaped interleaved and are set on a slightly different electric potential, called grid bias (GB). One anode is set to ground potential and referred to as collecting anode (CA) as it collects the generated electrons. The other is set on a negative potential of typically -40 V and is referred to as non-collecting anode (NCA). A bias voltage (BV) of typically $-1\,200\text{ V}$ is applied to the cathode. The detectors discussed in this publication are $(20 \times 20 \times 15)\text{ mm}^3$ in size with a volume of 6 cm^3 and a mass of 36 g . Their electrodes are configured according to a so-called coplanar quad-grid (CPqG), i.e. four individual CPG structures, rotated against each other by 90° . The whole CPqG structure is surrounded by a common guard ring (GR) which is left on a floating potential in a default configuration. Such a detector, but without a guard ring electrode, was characterized extensively in Ref. [14]. Details of the electrode design and its dimensions are depicted in Figure 1.

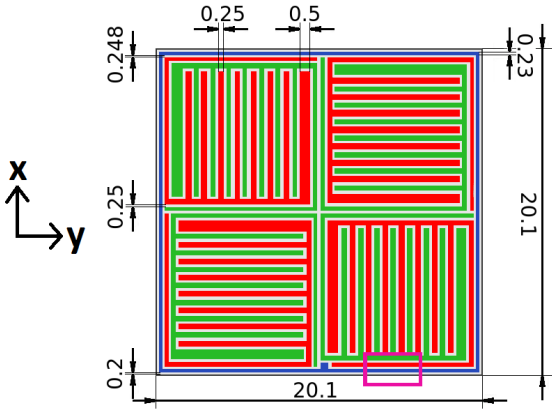


Figure 1. Scheme of the electrode configuration of a CPqG detector. The four sectors comprise individual CPGs, each instrumenting a collecting anode (CA, red) and a non-collecting anode (NCA, green). The surrounding guard ring (GR) is shown in blue. All distances are given in mm. The purple box indicates the position of the detailed view shown in Figure 2.

For the instrumentation of the guard ring a defined potential is set to it, in this case ground potential, which is the same potential as the CA. The guard ring can thus collect charges drifting to it. This is particularly important for charge clouds originating from interactions in the vicinity of the lateral detector surfaces. The anodes and the guard ring are connected to charge sensitive preamplifiers (Cremat CR110¹). These convert the induced charge signals coming from interactions in the detector volume into voltage signals. The signals are afterwards amplified in linear

¹<http://www.cremat.com/CR-110.pdf>

amplifiers and digitized in flash analog-to-digital converters (FADC SIS3300²) with a sampling rate of 100 MHz. The data contain the full pulse-shape information of the measured channels, so it is possible to apply pulse-shape analysis tools in the off-line analysis [9]. More details about the data-acquisition can be found in Ref. [6].

The deposited energy in a CPG detector can be reconstructed by calculating the amplitude A of the difference signal between the CA and NCA signal amplitudes including a so-called weighting factor w ,

$$E \propto A_{CA} - w \cdot A_{NCA}. \quad (2.1)$$

The weighting factor compensates for effects of electron trapping [13] and can be determined during the calibration process. The energy deposited in each CPqG sector can be reconstructed individually using Equation 2.1. The signal of the guard ring is not considered in the energy reconstruction in this study.

3 Charge-cloud dynamics of alpha particles

The penetration depth of alpha particles from radioactive decays in solids like CdZnTe is very short, about 20 μm for an alpha particle with a kinetic energy of 5 MeV. Therefore, events induced by sources of alpha radiation outside the detector volume deposit their energy in the vicinity of the surfaces and are referred to as lateral surface events. Due to the deposited energy, electron-hole pairs are created at the interaction point. The effect of holes is ignored here because their drift towards the cathode is much slower. The charge cloud of the generated electrons expands while drifting through the detector towards the electrodes due to two main reasons: mutual repulsion of the electrons as well as thermal diffusion. The maximal values for these two quantities can be calculated by considering near-cathode events in the detector. In this case, the created electron cloud drifts through the whole detector volume.

The spread σ_{diff} of the charge cloud due to diffusion [15] can be calculated as a function of the drift length x as

$$\sigma_{\text{diff}}(x) = \sqrt{\frac{2k_B T x}{eE}}, \quad (3.1)$$

where k_B is the Boltzmann constant, T the absolute temperature, e the electric elementary charge and E the electric field strength. At room temperature and with an applied BV of $-1\,200\text{ V}$ the resulting spread due to thermal diffusion for a maximal drift length of 15 mm is

$$\sigma_{\text{diff}}^{\text{max}} = \sigma_{\text{diff}}(15\text{ mm}) \approx 100\text{ }\mu\text{m}. \quad (3.2)$$

The expansion R_{rep} due to mutual repulsion is defined as the largest diameter of the charge cloud [16]. It can be calculated as function of the drift length to

$$R_{\text{rep}}(x) = \sqrt[3]{\frac{3eNx}{4\pi\epsilon_0\epsilon_r E}}, \quad (3.3)$$

with the number of created charge carriers N and the permittivity of free space and the relative permittivity, ϵ_0 and $\epsilon_r = 10.9$ [17], respectively. The energy of the alpha particles from the ^{241}Am

²<http://www.struck.de/sis3300.htm>

source is about 5.5 MeV, which is also typical for alpha particles from natural decay chains. In an interaction of this energy, about 10^6 charge carriers are produced. Therefore, the resulting spread due to repulsion is at most

$$R_{\text{rep}}^{\text{max}} = R_{\text{rep}}(15 \text{ mm}) \approx 420 \text{ } \mu\text{m}. \quad (3.4)$$

The quadratic sum of these two effects can be calculated to estimate an upper limit on the maximal spread L_{max} of a charge cloud [18, 19] assuming a maximal drift length of 15 mm for near-cathode events,

$$L_{\text{max}} = \sqrt{(\sigma_{\text{diff}}^{\text{max}})^2 + (R_{\text{rep}}^{\text{max}})^2} \approx 430 \text{ } \mu\text{m}. \quad (3.5)$$

An aspect not taken into account in this estimation is that the charge cloud is created directly next to the detector edge and therefore cannot expand equally in all directions.

The effect of the charge cloud expansion of alpha-induced lateral surface events on the electrodes is shown in Figure 2. The initial interaction has a distance of about $20 \text{ } \mu\text{m}$ from the surface. The expansion of the charge cloud is shown after a drift length of 1 mm, 3 mm, 6 mm, 10 mm and 15 mm. Even for the largest drift length of 15 mm, the outermost CPG anode (CA) is not affected by the charge cloud. Hence, a clear separation of alpha-induced lateral surface events and events occurring in the inner detector volume should be possible by instrumenting the guard ring.

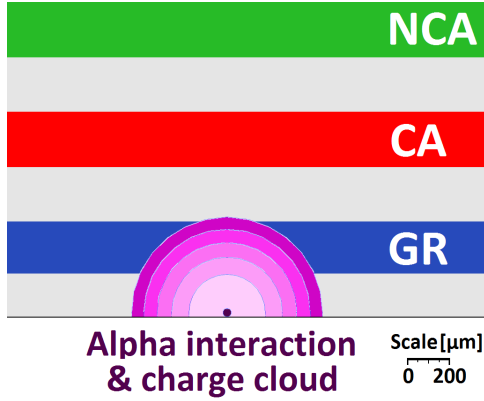


Figure 2. Detailed top view of the anode side as marked in Figure 1. The different types of magenta indicate the expansion of the charge cloud after a drift length of 1 mm, 3 mm, 6 mm, 10 mm and 15 mm. The dark dot highlights the initial charge cloud.

4 Predictions from an electric-field calculation

To study the effect of different guard ring potentials, e.g. floating potential in the default setting or ground potential for enabling charge collection, an electric-field simulation is performed using the simulation tool COMSOL Multiphysics in version 5.2 [20].

The current CPqG detector design is implemented in terms of dimensions and electrode design, the typical material-specific values for CdZnTe are taken from Ref. [21]. The applied bias voltage is assumed to be -1200 V and a typical value of -40 V is chosen for the GB. Configurations with different guard ring potential are simulated. In addition, the configuration of the CPqG anodes is varied: if a CA or an NCA bias is applied to the outermost anode, the configuration is referred to as CA_{out} and NCA_{out} mode, respectively. The simulated electric field-line distribution for the CA_{out} mode with the guard ring on ground potential is shown in Figure 3. Here, field lines start on the cathode in equidistant steps of $25 \text{ } \mu\text{m}$ and they end on the different electrodes (GR, CA and NCA

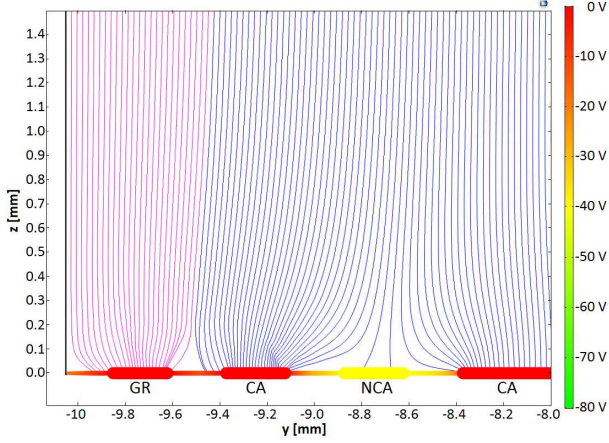


Figure 3. Electric field-line distribution shown in a cross section close to the detector edge. The guard ring is set on ground potential. The chosen GB and BV are -40 V and -1200 V. Field lines ending on the GR are colored in pink, those ending on the CPqG anodes in blue.

as highlighted). Field lines ending on the guard ring are colored in pink in contrast to field lines ending on either of the CPqG anodes, which are shown in blue.

The innermost field line ending on the guard ring starts at a distance of $625\text{ }\mu\text{m}$ from the detector edge. The maximal distance depends on the depth of the starting position, and a slope for the first 2 mm below the anode side is observed before the field lines are almost parallel. Energy deposited between the detector surface and the innermost field line ending on the guard ring will not be detected by the CA. This will lead to a decrease in the overall detection efficiency, but it will in particular suppress a large fraction of alpha-induced lateral surface events, according to Equation 3.5. The area influenced by the instrumented guard ring is visualized in Figure 4. This

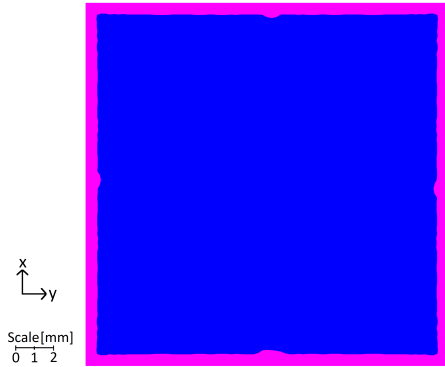


Figure 4. Contour plot of charge collection of the guard ring and the CPqG anodes in CA_{out} mode as seen from the top. Shown are the projected start positions of field lines finally ending on the guard ring (pink) or on either of the CPqG anodes (blue). The chosen GB is -40 V and BV is -1200 V.

contour plot depicts the start positions of electric field lines and differentiates between end positions on the guard ring electrode or the CPqG anodes. The dips in the area influenced by the CPqG at the middle of the sides arise from the transitions between the different CPG sectors. At the bottom, the dip is larger because of the guard ring contact pad. The ratio of the area influenced by the guard ring relative to the full area is a measure of reduction of the fiducial detector volume, ϵ_{fid} . The results for the CA_{out} mode, as depicted in Figure 4, and for the NCA_{out} mode are

$$\epsilon_{\text{fid}}^{\text{CA}_{\text{out}}} = 87.7\% \quad \text{and} \quad \epsilon_{\text{fid}}^{\text{NCA}_{\text{out}}} = 86.0\%, \quad (4.1)$$

respectively. The uncertainties in these calculations are negligible as the mesh for the numerical calculation is fine ($25\text{ }\mu\text{m}$), and small variations of the biases do also not show a notable effect.

Only the CA_{out} mode is evaluated in the following because of the expected larger efficiency than in NCA_{out} mode. In addition, other beneficial effects like less charge-sharing between the sectors favor this mode.

5 Experimental setup

The effect of instrumenting the guard ring in terms of a suppression of alpha interactions from the lateral surfaces is studied in measurements. A prototype CPqG detector with guard ring, produced by Redlen Technologies³, is used. During characterization of this test detector, the energy resolution in terms of full-width at half maximum (FWHM) for an incident energy of 662 keV of the different CPG sectors is measured. Two of the four sectors have only poor energy resolutions of 5.0 % and 7.0 %. Another sector is suffering of leakage currents degrading its performance immensely, while not influencing the other sectors. Finally, the last remaining sector provides a satisfactory energy resolution of 3.0 %. This sector is therefore chosen as the sector for testing.

A ^{241}Am source emitting alpha particles with an energy of 5.5 MeV is used to provide a sample of alpha-induced surface interactions. The source is pointed directly on the sector under test. Furthermore, the detector can be irradiated with gamma radiation from a ^{232}Th source with various gamma lines, the highest at an energy of 2 614 keV. In this case the whole detector is irradiated almost homogeneously.

The detector is mounted on a movable stage, so that it is possible to irradiate the detector at first with gamma radiation and afterwards with the alpha source without switching off the biases when exchanging the sources. Hence, the recorded gamma energy spectrum can be used for a common calibration for each configuration. The measurement setup as well as the tested sectors are depicted in Figure 5.

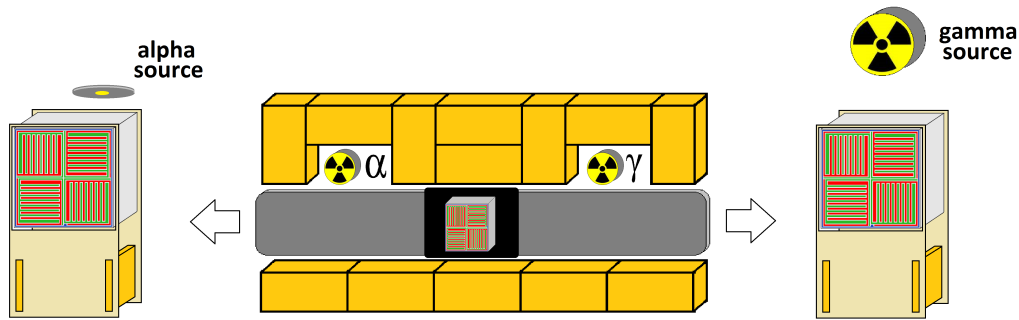


Figure 5. Top view of the measurement setup for evaluating the effect of the guard-ring instrumentation. The detector is mounted on a movable stage allowing to shift it between the two different radioactive sources (α : ^{241}Am source, γ : ^{232}Th source). The alpha source is pointed to the sector under test, whereas the gamma source irradiates the whole detector. The yellow bricks symbolize lead shielding.

To account for background, a dedicated measurement of the background spectrum is performed. The detector is kept in the same position as for an alpha measurement, but the ^{241}Am source is removed. Only background events originating from the natural laboratory background, cosmic muons or scattered photons from the ^{232}Th gamma source are recorded.

³<http://redlen.ca/>

To evaluate the effect of the instrumented guard ring, one measurement is performed with the guard ring on ground potential and one with the guard ring kept on a floating potential. The applied voltages for this measurement campaign are a GB of -40 V and a BV of -1 200 V.

6 Measurements and results

The energy spectra of the sector under test irradiated with ^{232}Th gamma radiation are shown in Figure 6. The reconstructed energy spectrum for the case of a floating guard ring is depicted in blue and for the case of an instrumented guard ring in red. The sharp drop around 280 keV stems from the threshold for the energy reconstruction needed for event-by-event triggering. The spectrum shows the typical features of a ^{232}Th source. The total event rate in the case of an instrumented guard ring is reduced compared to the floating case due to the reduced efficiency. This is expected from the results of the electric-field calculation in section 4.

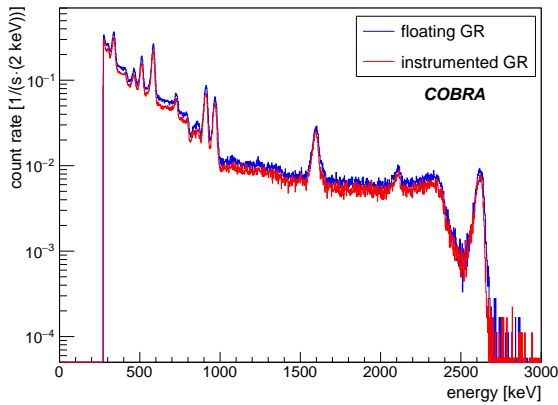


Figure 6. ^{232}Th energy spectra measured with the sector under test. Shown are the cases of floating (blue) and instrumented guard ring (red).

For the alpha measurement, the resulting energy spectra for both guard ring configurations are shown in Figure 7. The unusual spectral shape of the alpha spectrum for the floating guard ring can be explained by the attenuation due to air between the source and detector, and the detector surface encapsulation, especially as the source is not collimated and effects of the solid angle occur. This results in a smeared distribution shifted towards lower energies. The spectrum of alpha-induced lateral surface events in the instrumented guard ring configuration is clearly reduced compared to the floating potential case.

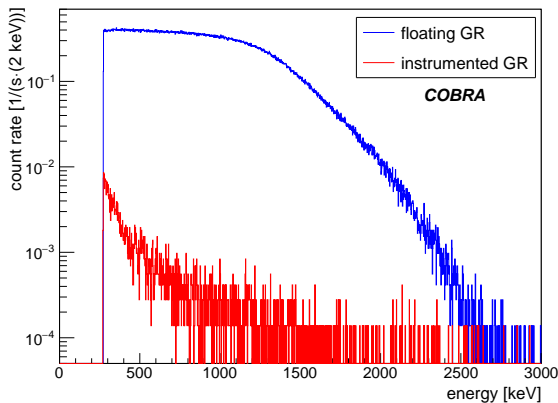


Figure 7. ^{241}Am energy spectra measured with the sector under test. Shown are the cases of floating (blue) and instrumented guard ring (red).

The spectra resulting from dedicated measurements of the laboratory background are shown in Figure 8. One can see similar spectra for both configurations of the guard ring again. This is expected because most background events stem from gamma radiation and muons. A large fraction of the events in the spectrum from the alpha measurement with an instrumented guard ring (red curve in Figure 7) are caused by laboratory background, which needs to be considered when estimating the suppression of alpha-induced events.

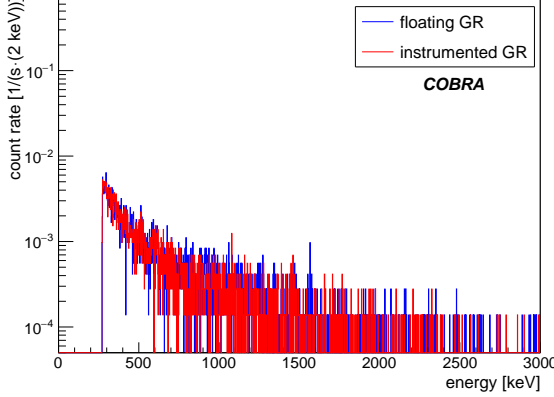


Figure 8. Background energy spectra measured with the sector under test. Shown are the cases of floating (blue) and instrumented guard ring (red).

This is evaluated quantitatively in Table 1 for all six measurements by comparing the count rates, integrated between 280 keV and 3 000 keV. The quoted uncertainties are due to the statistical Poisson error.

Table 1. Results of measurements for sector under test. Given are the integral count rates r (between trigger threshold and chosen high energy cut-off) in each measurement and for both guard ring configurations.

		alpha measurement	background measurement	gamma measurement
$r_{\text{floating GR}}$	[1/s]	208.6 ± 0.2	0.493 ± 0.008	42.33 ± 0.05
$r_{\text{instrumented GR}}$	[1/s]	0.498 ± 0.008	0.465 ± 0.008	36.15 ± 0.04

The resulting reduction of the fiducial volume for gamma radiation in the case of an instrumented guard ring is estimated as

$$\epsilon_{\gamma} = \frac{r_{\text{instrumented GR}}^{\gamma} - r_{\text{instrumented GR}}^{\text{bkg}}}{r_{\text{floating GR}}^{\gamma} - r_{\text{floating GR}}^{\text{bkg}}}. \quad (6.1)$$

Using the numbers in Table 1, this yields

$$\epsilon_{\gamma} = (85.3 \pm 0.1) \%. \quad (6.2)$$

This value is comparable with the prediction of $\epsilon_{\text{fid}} = 87.7 \%$ from the calculation of the electric field (Equation 4.1). The differences arise from effects of a real detector that are not incorporated in the electric-field calculation, e.g. inhomogeneities in the detector bulk, uncertainties in the electrode placements or the energy resolution.

The suppression factor for alpha-induced lateral surface events SF_α can be defined as

$$SF_\alpha = \frac{r_{\text{floating GR}}^\alpha - r_{\text{floating GR}}^{\text{bkg}}}{r_{\text{instrumented GR}}^\alpha - r_{\text{instrumented GR}}^{\text{bkg}}}. \quad (6.3)$$

As the rates in the numerator and the denominator differ by about four orders of magnitude, common Gaussian uncertainty propagation cannot be used for the calculation of the ratio. Instead, the suppression factor is estimated based on a toy Monte-Carlo study: 10^7 pairs of random numbers are drawn from two Gaussian distributions, characterized by the numerator and the denominator, and the resulting frequency distribution of the ratios of these numbers is interpreted as the probability density of SF_α . Because this asymmetric distribution features a strong non-Gaussian tail towards larger values, the suppression factor is estimated by the mode of the distribution. The smallest interval containing 68.3 % of all entries is interpreted as the uncertainty interval. This yields

$$SF_\alpha = 5300_{-1380}^{+2660}. \quad (6.4)$$

This is a large improvement compared to the pulse-shape analysis currently used to suppress lateral surface events in COBRA [8, 9]: the relative detection efficiency for gamma radiation is about the same, but the suppression factor for alpha-induced lateral surface events is nearly three orders of magnitude larger.

7 Summary and outlook

The COBRA collaboration searches for neutrinoless double beta-decay and hence background reduction is a crucial issue. Alpha-induced lateral surface events are the main background source when operating the COBRA demonstrator. In this paper, dedicated laboratory measurements and calculations of electric fields are used to demonstrate that instrumenting the guard ring of CPqG detectors leads to a suppression factor for alpha-induced lateral surface events of 5300_{-1380}^{+2660} , while the reduction of fiducial volume for gamma events occurring throughout the entire detector volume is $(85.3 \pm 0.1) \%$.

This concept will be followed in the upgrade of the COBRA extended demonstrator (XDEM). Under optimal conditions and the assumption that the background is dominated by alpha events, the overall background rate is expected to be lowered by two orders of magnitude.

The signals of the guard ring are measured, but not included in the analysis presented here. A modified event reconstruction including the guard-ring signal can in principle be performed. Preliminary studies indicate that using this additional information is feasible and can improve the detector performance (e.g. the detection efficiency) and the veto capabilities for lateral surface events even further.

Acknowledgments

We thank the LNGS for the continuous support of the COBRA experiment. COBRA is supported by the German Research Foundation DFG (ZU 123/15-1 / GO 1133/3-1). Furthermore, we thank COMSOL for support with the COMSOL Multiphysics simulation and O. Schulz for technical support with the DAQ.

References

- [1] K. Zuber. COBRA: Double beta decay searches using CdTe detectors. *Phys. Lett. B*, 519:1–7, 2001.
- [2] W. H. Furry. On Transition Probabilities in Double Beta-Disintegration. *Phys. Rev.*, 56:1184, 1939.
- [3] M. Agostini et al. Limit on Neutrinoless Double Beta Decay of ^{76}Ge by GERDA. *Phys. Procedia*, 61:828–837, 2015.
- [4] K. Asakura et al. Results from KamLAND-Zen. *AIP Conf. Proc.*, 1666:170003, 2015.
- [5] C. Alduino et al. Analysis techniques for the evaluation of the neutrinoless double- β decay lifetime in ^{130}Te with the CUORE-0 detector. *Phys. Rev. C*, 93:045503, 2016.
- [6] J. Ebert et al. The COBRA demonstrator at the LNGS underground laboratory. *Nucl. Instrum. Meth. A*, 807:114–120, 2016.
- [7] S. Rahaman et al. Double-beta decay Q values of ^{116}Cd and ^{130}Te . *Phys. Lett. B*, 703:412–416, 2011.
- [8] J. Ebert et al. Results of a search for neutrinoless double- β decay using the COBRA demonstrator. *Phys. Rev. C*, 94:024603, 2016.
- [9] M. Fritts et al. Pulse-shape discrimination of surface events in CdZnTe detectors for the COBRA experiment. *Nucl. Instrum. Meth. A*, 749:27–34, 2014.
- [10] Z. He et al. Coplanar grid patterns and their effect on energy resolution of CdZnTe detectors. *Nucl. Instrum. Meth. A*, 411(1):107–113, 1998.
- [11] A. Broniatowski et al. A new high-background-rejection dark matter Ge cryogenic detector. *Phys. Lett. B*, 681(4):305–309, 2009.
- [12] J. Tebrügge. *Commissioning of the COBRA demonstrator and investigation of surface events as its main background*. PhD thesis, TU Dortmund, 2016. arXiv: 1609.03783.
- [13] P. N. Luke. Single-polarity charge sensing in ionization detectors using coplanar electrodes. *Appl. Phys. Lett.*, 65(22):2884–2886, 1994.
- [14] J. Ebert et al. Characterization of a large CdZnTe detector with a coplanar quad-grid design. *Nucl. Instrum. Meth. A*, 806:159–168, 2016.
- [15] Knoll, G. F. *Radiation Detection and Measurement*, 4th ed. John Wiley and Sons, 2010.
- [16] E. Gatti et al. Dynamics of electrons in drift detectors. *Nucl. Instrum. Meth. A*, 253(3):393–399, 1987.
- [17] Capper, P. *Properties of narrow gap cadmium based compounds*. Institution of Engineering and Technology, 1994.
- [18] B. Donmez et al. Continued studies of single-sided charge-sharing CZT strip detectors. In *IEEE Nucl. Sci. Symp. Conf. Rec.*, volume 3, pages 1408–1411, 2005.
- [19] M. Benoit and L. A. Hamel. Simulation of charge collection processes in semiconductor CdZnTe γ -ray detectors. *Nucl. Instrum. Meth. A*, 606(3):508–516, 2009.
- [20] COMSOL Inc. COMSOL Multiphysics. <http://www.comsol.com/>. Online source; accessed 11-December-2016.
- [21] Q. Zhang et al. Progress in the Development of CdZnTe Unipolar Detectors for Different Anode Geometries and Data Corrections. *Sensors*, 13(2):2447, 2013.